Assessment of MOCVD- and MBE-Grown GaAs for High-Efficiency Solar Cell Applications

STEPHEN P. TOBIN, MEMBER, IEEE, S. M. VERNON, C. BAJGAR,
STEVEN J. WOJTCZUK, MEMBER, IEEE, MICHAEL R. MELLOCH, MEMBER, IEEE,
A. KESHAVARZI, T. B. STELLWAG, S. VENKATENSAN,
MARK S. LUNDSTROM, MEMBER, IEEE, AND
KEITH A. EMERY, MEMBER, IEEE

Abstract—**A critical assessment of the photovoltaic quality of epitaxial GaAs grown by metal-organic chemical vapor deposition (MOCVD) and by molecular-beam epitaxy (MBE) is reported. Epitaxial films of nominally identical structure were grown by the two techniques and were fabricated into p-n heteroface solar cells. The 0.5-cm by 0.5-cm cells were then characterized and compared. The MOCVD-grown films produced independently verified record efficiency cells of 24.8 percent under 1-sun AM1.5 global conditions while the MBE-grown films produced similarly high efficiencies of 23.8 percent. The material quality of the two films in terms of minority-carrier diffusion lengths and surface recombination velocities were quite comparable. These results demonstrate that the quality of MBE-grown films can be quite comparable to the best MOCVD-grown films and that they are suitable for high-efficiency solar cells.**

I. Introduction

THE efficiency of GaAs solar cells continues to rise as device designs are optimized, material quality improves, and device processing improves [1]–[3]. To date, the best performance has been achieved for cells fabricated on films grown by metal-organic chemical vapor deposition (MOCVD), but molecular-beam epitaxy (MBE) has also been used in research [4], [5]. MBE is a useful tool for advanced cell research because of the relative ease with which sophisticated heterostructures can be grown. It has also proven useful for basic studies of minority-carrier injection, transport, and recombination in GaAs-based cells [6], [7]. The efficiencies obtained from cells using MBE-grown films, however, has been considerably less than that for MOCVD-grown films. For example, the highest reported AM1.5 global efficiency for an MBE cell is 15.7 percent (projected to 21 percent with an anti-reflection coating) [5], while MOCVD-grown cells have achieved efficiencies of 24.5 percent [1]. As a result, there is a concern that research results obtained from MBE-grown films might not be applicable to the more widely used MOCVD technology.

Our purpose in this paper is to critically assess the performance of high-efficiency solar cells fabricated on MBE-grown epitaxial films. MOCVD- and MBE-grown films were processed together into high-efficiency 0.5-cm by 0.5-cm solar cells (see Fig. 1). We found that the important cell parameters (i.e., emitter and base diffusion lengths and heteroface recombination velocity) are quite comparable for the two technologies. The 24.8-percent efficiencies achieved in this study for the MOCVD-grown cells are the highest reported under 1-sun AM1.5 conditions for any single-junction cell. The MBE-grown films produced a slightly lower (23.8-percent) efficiency, which is, however, a record for MBE-grown films.

II. Experimental Methods

A. Molecular-Beam Epitaxy System Preparation and Growth Procedure

The MBE films were grown in a new 3-in modular-Varian GEN II MBE at Purdue University. (This MBE system has already produced extremely high-electron-mobility modulation-doped heterojunctions [8].) The growth chamber, without source furnaces, was baked at 200°C for 3 days. The source furnaces, and then the furnaces with their pyrolytic boron nitride crucibles, were baked in a separate vacuum chamber before placement into the growth chamber. The furnaces were then baked in the growth chamber followed by loading of source material. The arsenic source was a 99.99999-percent pure arsenic slug, the gallium source was 99.999999 percent pure, the aluminum source was 99.9999 percent pure, the beryllium source was 99.999 percent pure, and the silicon source came from a high-purity crystalline wafer. The MBE system was baked for 3 days at 200°C after loading sources.

Following the initial loading of source material, 32 films were grown before the two MBE films used in this work. One film was grown on a 2-in n^+GaAs liquid-encapsulated Czochralski (LEC) wafer (film 120988A), while the other film was grown on a 2-in n^+GaAs hori-

Manuscript received April 30, 1989; revised October 2, 1989. This work was supported by the Solar Energy Research Institute for the U.S. Department of Energy under Contracts XL-8-18063-1 (Spire Corporation) and XL-5-05018-1 (Purdue University).

S. P. Tobin, S. M. Vernon, C. Bajgar, and S. J. Wojtczuk are with the Spire Corporation, Patriots Park, Bedford, MA 01730.

M. R. Melloch, A. Keshavarzi, T. B. Stellwag, S. Venkatensan, and M. S. Lundstrom are with Purdue University, East Lafayette, IN 47907.

K. A. Emery is with the Solar Energy Research Institute, Golden, CO 80401.

IEEE Log Number 8932675.

0018-9383/90/0200-0469$01.00 © 1990 IEEE

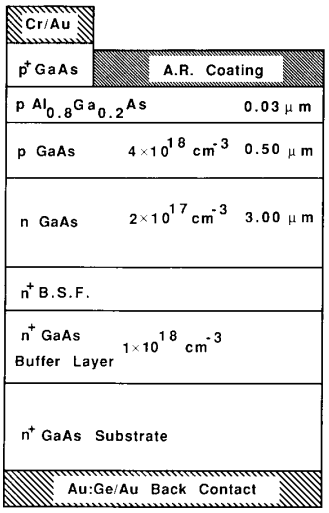

Fig. 1. Nominal GaAs solar cell structure.

zontal Bridgman wafer (film 121588B). The wafers were degreased, etched for 1 min in a 60°C solution of 5 : 1 : 1 $H_2SO_4 : H_2O_2 : H_2O$, rinsed in deionized H_2O, and placed in a nonindium wafer mount. The samples were then loaded on their carrying trolley and placed into the entry chamber of the MBE system, where they were outgassed for 2 h at 200°C. The trolley was then placed into the buffer chamber where the samples were outgassed on a heater station at 300°C for 1 h immediately prior to being introduced into the growth chamber. Liquid nitrogen was circulated through the cryoshrouds starting about 2 h before initiating growth. (Note that the source furnaces are maintained at 200°C except for the arsenic source, which is maintained at 100°C when the MBE system is idle.)

All the MBE layers were grown at a substrate temperature of 600°C (580°C is the oxide desorption temperature), and the wafers were rotated at 5 r/min during most of the film growth. The film growth rates were determined from monitoring the intensity of the specular spot of the reflection high-energy electron diffraction pattern [9]. All layers were grown at a rate of 1.0 μm/h except for part of the back surface field (BSF) layer (see Fig. 1). At a GaAs growth rate of 1 μm/h, the As_4 to Ga beam equivalent pressure was 20 as determined by an ion gauge placed in the substrate growth position. The BSF layer consisted of a 20-period superlattice of 28-Å $Al_{0.36}Ga_{0.64}As$ barriers and 27-Å GaAs wells. (The $Al_{0.36}Ga_{0.64}As$ barriers were grown at a rate of 1.0 μm/h and the GaAs wells at 0.64 μm/h.) The BSF field layer acts as a barrier to minority-carrier holes in the n-GaAs region, which increases the probability of their collection across the p-n junction. A superlattice was used for this purpose rather than just a thick AlGaAs region since, in MBE, a GaAs region grown on a superlattice exhibits a better electrical interface than when a GaAs region is grown on a thick AlGaAs region [10], [11].

B. Metal-Organic Chemical Vapor Deposition Growth Procedure

The MOCVD films were grown in a Spire Corporation SPI-MO CVD™ 450 epitaxial reactor at Spire Corporation. This is a vertical-geometry barrel-type reactor operating at atmospheric pressure. Five 2-in n^+GaAs horizontal Bridgman substrate wafers were used in each deposition run. Trimethylgallium, trimethylaluminum, and arsine were the source gases, with silane and dimethylzinc diluted in hydrogen used for n- and p-type dopants. In the first run (15271), the active layers were grown at 740°C, and in the second run (15523), the active layers were grown at 775°C. In both cases, the growth temperature was lowered to 700°C in the GaAs cap layer to achieve a high p^+ doping level for low-resistance nonalloyed contacts (see Fig. 1). The GaAs and AlGaAs layers were grown at a rate of 4 μm/h. The group V to group III flow ratios were 15 at 740°C and 20 at 775°C.

The structure of the MOCVD cells was nominally the same as that of the MBE cells except for the BSF layer. The MOCVD cells used a 1-μm layer of $Al_{0.3}Ga_{0.7}As$ instead of a superlattice.

C. Device Processing

Two MOCVD and two MBE wafers were processed together as a batch. The post-growth device processing sequence has been described previously [12]; a brief summary follows. First, the wafer front was coated with SiO_2. Next, a thin AuGe back ohmic contact layer was evaporated and alloyed, followed by an evaporated Au back metallization. Image-reversal photolithography was used to form a pattern for front grid metallization [13]. After etching SiO_2 in the grid openings, Cr and Au were evaporated for front contacts. The photoresist was dissolved to lift off excess metal; then the contacts were sintered. Photolithography was used to define a pattern for mesa etch (0.5-cm by 0.5-cm junctions); then a phosphoric-acid-based etchant was used to form the mesa. All remaining SiO_2 was removed just prior to a selective cap removal etch (ammonium hydroxide-hydrogen peroxide system). The etch removed the GaAs cap layer everywhere except under the grid lines and exposed the AlGaAs window layer. Finally, a double-layer antireflection coating of ZnS and MgF_2 was thermally evaporated.

D. Device Characterization

The solar cell conversion efficiency was measured at Spire Corporation under AM1.5 global conditions using a Spectrolab X-25 solar simulator and a silicon reference cell calibrated by the Solar Energy Research Institute (SERI). A spectral mismatch correction on the order of 1 percent was applied. The short-circuit current value was verified by integrating the measured absolute external quantum efficiency with the reference AM1.5 global spectrum [14]. Efficiency measurements were verified by SERI using standard test procedures [15].

Absolute spectral response and specular reflectance measurements were made simultaneously using a monochromator system from Optronic Laboratories. An NBS-traceable calibrated silicon photodiode was used as the spectral response standard and a clean silicon wafer was used as the reflectance standard. Measurements were made under dc conditions with no light bias. The measured cell reflectance was corrected for grid reflectance to give the reflectance R of the nonmetallic surface. The internal quantum efficiency was then determined by dividing the external quantum efficiency by $(1 - R)(1 - S)$, where S is the grid shadow, defined as the ratio of metallized area to total cell area.

The forward dark log I–V characteristics and the log I_{sc}–V_{oc} characteristics were measured using a current source, voltmeter, and an ELH lamp with a variable power supply.

Doping profiles in the epitaxial wafers were measured by electrochemical C–V profiling [16]. Doping concentrations on the n-side were also measured by junction capacitance and on the p-side by sheet resistance using the transmission line method. Thicknesses of the cap, window, and antireflection coating layers and compositions of the AlGaAs window layers were measured by optical reflectance spectroscopy [17].

III. Results

A. Structural Characterization

The dopings and thickness of the epitaxial layers were close to the target values for both growth techniques. Structural characterization results are summarized in Table I. In the table, optical reflectance spectroscopy (ORS) was used to determine the window thickness and composition. The other values were determined from electrochemical C-V (ECV) profiling. Excellent agreement (a less than 100-Å difference) was observed between the ORS and ECV thicknesses of the cap and window layers. The ECV dopings and thicknesses of the cap and emitter layers were also consistent with the sheet resistances of these layers.

Growth defects were readily observed with an optical microscope in the as-grown MBE material. Oval defects of types A and B [18] were both present with total densities of 500 cm^{-2} in wafer 120988A and 1000 cm^{-2} in wafer 121588B. Stacking faults at a density of 1×10^4 cm^{-2} were observed only in wafer 120988A. Their size indicated that they originated near the substrate–epitaxial layer interface. These types of defects were not present in MOCVD-grown films.

B. Conversion Efficiency

Table II summarizes the efficiency averages and standard deviations for each of the four wafers. The statistics include *all* processed cells on the wafers. Removing one or two low-efficiency cells from each wafer lowered the standard deviation of efficiency to 1.4 and 1.2 percent of the mean for the MOCVD wafers, and to 1.7 and 4.7 percent of the mean for the MBE wafers. The uniformity of efficiency was therefore excellent across the wafers in most cases. Wafer maps of efficiency are shown in Figs. 2 and 3. For the MBE films, half of each wafer was used for solar cell processing and half for diagnostic measurements. For the MOCVD films, a full wafer was used for solar cells and another wafer from the same growth run was used for diagnostics. It can be seen that both growth techniques produced very high efficiency cells, with 25.1 percent for the best MOCVD cell and 23.7 percent for the best MBE cell. Confirming measurements at SERI were in good agreement, with 24.8 percent for the best MOCVD cell and 23.8 percent for the best MBE cell. SERI's measurements are summarized in Table III, and the I–V curve of the best cell is shown in Fig. 4. SERI also measured the best cells under AM0 conditions (see Table III), with the best efficiency being 21.7 percent.

TABLE I
STRUCTURAL CHARACTERIZATION OF THE SOLAR CELL EPITAXIAL LAYERS
(Thicknesses are in micrometers and dopings are in reciprocal cubic centimeters. Dashes indicate no measurement.)

Wafer	Cap		$Al_xGa_{1-x}As$ Window			Emitter		Base	
	Thick.	Doping	Thick.	Doping	x	Thick.	Doping	Thick	Doping
Target Values	0.35	4×10^{19}	0.03	1×10^{18}	0.80	0.50	4×10^{18}	3.0	2×10^{17}
15271	0.35	4×10^{19}	0.027	4×10^{18}	0.81	0.56	4×10^{18}	3.0	1.7×10^{17}
15523	0.38	4×10^{19}	0.030	1×10^{18}	0.83	0.66	3×10^{18}	3.6	2.0×10^{17}
120988A	0.37	1×10^{19}	0.036	5×10^{18}	0.72	0.52	3×10^{18}	3.0	1.5×10^{17}
121588B	0.39	-	0.034	-	0.69	-	-	3.0	1.4×10^{17}

TABLE II
COMPARISON OF WAFER AVERAGES OF EFFICIENCY FOR THE MOCVD VERSUS MBE COMPARISON
(AM1.5 Global, 100 mW/cm^2, 25°C, 0.250 cm^2, total area. Standard deviations in parentheses.)

Growth Technique	Wafer ID	Voc (V)	Jsc (mA/cm^2)	FF (%)	Eff (%)	# of Cells
MOVCD	15271	1.024 (0.002)	27.56 (0.25)	86.3 (1.2)	24.34 (0.43)	39
MOCVD	15523	1.027 (0.024)	27.62 (0.17)	86.0 (1.5)	24.40 (0.93)	40
MBE	120988A	1.019 (0.005)	27.41 (0.13)	82.9 (1.4)	23.14 (0.42)	15
MBE	121588B	0.987 (0.059)	27.40 (0.34)	81.4 (2.0)	22.03 (1.57)	24

C. Optical Characterization

The internal quantum efficiencies for one cell on each wafer are shown in Fig. 5. Peak internal quantum efficiencies are nearly 1, within our measurement accuracy, for both types of cells, indicating long minority-carrier diffusion lengths and very good AlGaAs–GaAs interfaces. The long-wavelength response is similar for all cells, indicating similar diffusion lengths in the n-type base layer. The response of the MBE cells at wavelengths below 550 nm is a little lower than that of the MOCVD cells because the windows are a little thicker and the AlAs fraction (x) in $Al_xGa_{1-x}As$ is lower. Reflectance curves for each of the cells and our resulting analysis of the AR

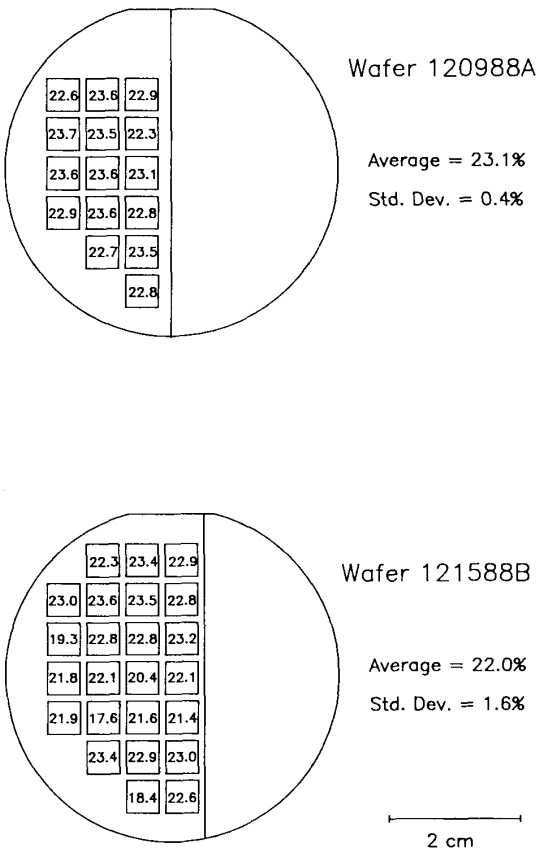

Fig. 2. Efficiency maps (AM1.5 global, 1 sun, 25°C) for the two MBE wafers.

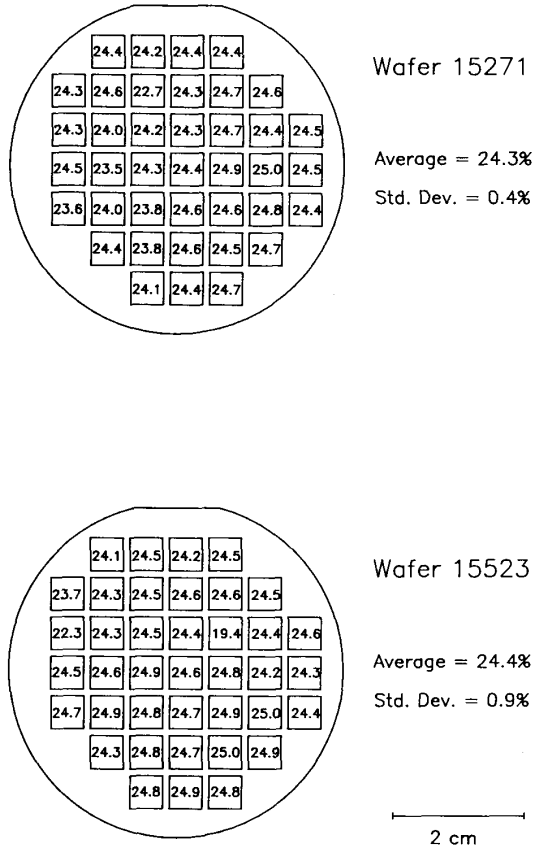

Fig. 3. Efficiency maps (AM1.5 global, 1 sun, 25°C) for the two MOCVD wafers.

and window layer thicknesses using ORS are shown in Fig. 6. As a point of reference, the theoretically optimum AR thicknesses are roughly 1000 Å for MgF_2 and 500 Å for ZnS. The MgF_2 thicknesses were off from the target value by about 15 percent for wafers 15523 and 120988A, but this only gives about a 0.15-mA/cm^2 loss in short-circuit current density relative to the optimum AR. The other two wafers were much closer to the ideal case. Grid shadow was 4.9 percent in all cases.

D. Junction Characterization

Fig. 7 compares the forward log J–V characteristics of one cell from each wafer. (The J_{sc}–V_{oc} characteristics are plotted to avoid series resistance effects at the highest current levels. Below 1×10^{-2} A/cm^2, the dark J–V characteristics coincided with J_{sc}–V_{oc}.) At current levels corresponding to 1-sun illumination, all cells are limited by diffusion current with ideality factor $n = 1$. At lower current levels, the MOCVD cells are limited by $n = 2$ space-charge recombination current while the MBE cells are limited by a nonideal leakage current with $2.1 \leq n \leq 2.6$. The higher excess current in the MBE cells is responsible for their lower fill factors relative to the MOCVD cells. Results of fitting the log J–V characteristics to the standard double-exponential model

$$J = J_{o1}(\exp[qV/kT] - 1) + J_{o2}(\exp[qV/n_2kT] - 1) \quad (1)$$

are listed in Table IV. For the MOCVD cells, a two-parameter fit (J_{o1} and J_{o2}) with $n_2 = 2.0$ gave a very good fit to the data, while the MBE cells required a three-parameter fit (J_{o1}, J_{o2}, and n_2) with $n_2 > 2.0$. Similar dif-

TABLE III
EFFICIENCY MEASUREMENTS MADE AT SERI FOR THE BEST CELL FROM EACH WAFER
(Test conditions: 25°C, 0.250 cm^2, total area. AM1.5 = global spectrum, 1000 W/m^2; AM0 = 1367 W/m^2.)

Growth Method	Wafer #	Cell #	Test Conditions	Voc (V)	Jsc (mA/cm^2)	FF (%)	Eff (%)
MOCVD	15271	18	AM1.5	1.021	27.67	86.36	24.4
MOCVD	15523	5	AM1.5	1.029	27.89	86.43	24.8
MBE	120988A	14	AM1.5	1.026	27.12	84.62	23.5
MBE	121588B	22	AM1.5	1.018	27.56	84.65	23.8
MOCVD	15523	5	AM0	1.033	33.11	86.70	21.7
MBE	121588B	22	AM0	1.022	32.79	84.67	20.8

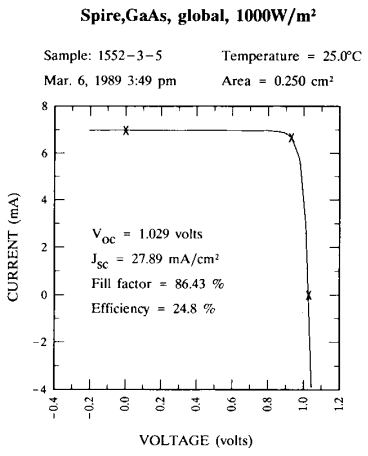

Fig. 4. AM1.5 efficiency curve measured by SERI for the 24.8-percent efficient GaAs cell.

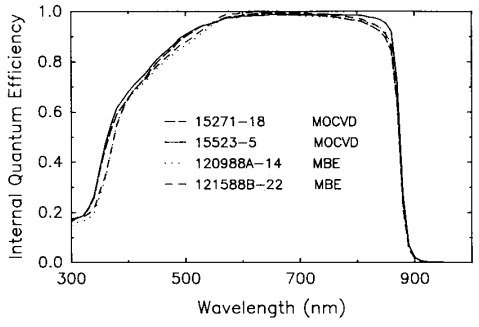

Fig. 5. Comparison of internal quantum efficiencies for MBE and MOCVD solar cells.

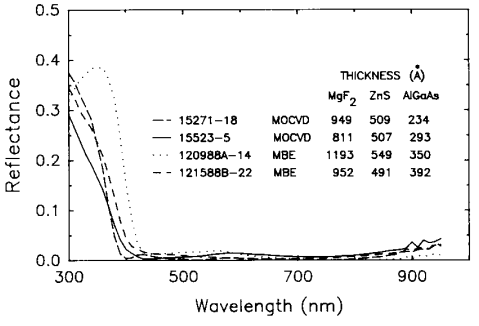

Fig. 6. Comparison of specular surface reflectances (no grid lines) for MBE and MOCVD solar cells.

fusion saturation currents (J_{o1}) were found for MOCVD and MBE cells, indicating similar minority-carrier diffusion lengths and interface recombination velocities. The lowest diffusion saturation currents were from MOCVD run 15523.

A series of mesa-isolated diodes with areas ranging from 2.5×10^{-5} to 0.01 cm^2 was fabricated on the same

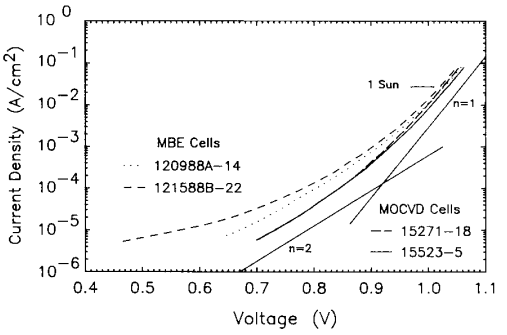

Fig. 7. Comparison of log J-V characteristics for MBE and MOCVD solar cells.

TABLE IV
RESULTS OF CURVE-FITTING THE MEASURED log J-V CHARACTERISTICS OF 0.5 cm × 0.5 cm SOLAR CELLS TO (1)

Growth Method	Cell #	J_{o1} (A/cm²)	J_{o2} (A/cm²)	n_2
MOCVD	15271-18	1.13×10^{-19}	5.82×10^{-12}	2.00
MOCVD	15523-5	7.98×10^{-20}	6.22×10^{-12}	2.00
MBE	120988A-14	9.30×10^{-20}	3.77×10^{-11}	2.12
MBE	121588B-22	1.32×10^{-19}	6.96×10^{-10}	2.54

wafers as the solar cells. Of the MBE diodes, only a few of the largest 0.01-cm^2 diodes exhibited the $n > 2$ shunt leakage exhibited by *all* of the 0.25-cm^2 MBE solar cells. The correlation between the $n > 2$ leakage current and diode area indicates that the leakage is due to isolated defects.

The $n = 2$ dark current of GaAs solar cells is comprised of components due to recombination in the bulk space-charge region and within the space-charge region exposed at the perimeter of the mesa. Writing the $n = 2$ saturation current as

$$I_{o2} = J_{o2B}A + J_{o2P}P \tag{2}$$

(where J_{o2B} is the bulk component (in amperes per square centimeter), J_{o2P} the perimeter component (in amperes per centimeter), A the area, and P the perimeter) shows that the bulk and perimeter components can be extracted by plotting I_{o2}/A versus perimeter-to-area ratio. The series of mesa-isolated diodes described above had P/A ratios varying from 40 to 800 cm^{-1}. From the measured dark current–voltage characteristic, the $n = 2$ current was extracted by curve fitting to (1), and the results are plotted in Fig. 8.

The results displayed in Fig. 8 confirm an earlier analysis that demonstrated that the dominant $n = 2$ current component arose from perimeter recombination [19]. The fact that the bulk current component is very small for both films indicates that bulk space-charge-recombination lifetimes of both the MOCVD- and MBE-grown films are high. Fig. 8 shows a somewhat lower $n = 2$ bulk component (J_{o2} axis intercept) for the MOCVD film, suggesting that the recombination lifetime may be higher for

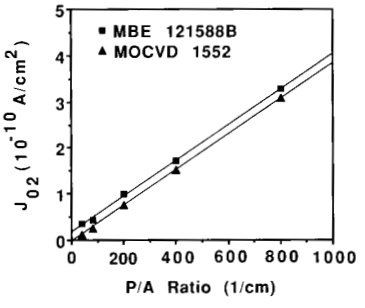

Fig. 8. Plot of the extracted J_{o2} current component versus perimeter to area ratio for diodes fabricated on MOCVD-grown (#15523) and MBE-grown (#121588B) films. The measurement temperature was 26°C.

this material. However, not enough measurements were made to form a definite conclusion.

The $n = 2$ perimeter current density can be expressed as [20]

$$J_{o2P} = qn_i(S_{SCR}L_s) \tag{3}$$

where S_{SCR} is the surface recombination velocity in the exposed space-charge region, and L_s is the so-called surface diffusion length [20]. Using n_i (26°C) from Blakemore [21] and the data plotted in Fig. 8, we find $(S_{SCR}L_s) = 1.2$ cm^2/s for both the MOCVD-grown film 15523 and for the MBE-grown film 121588B. This value is consistent with [20] for freshly prepared surfaces. For the MOCVD-grown 0.5-cm × 0.5-cm solar cells, the measured $n = 2$ saturation current was quite close to the 0.7×10^{-12} A predicted from (3), n_i at 25°C, and the measured $S_{SCR}L_s$ product. This indicates that, even for 0.25-cm^2 cells, the perimeter current is dominant over the bulk. At 25°C, the average measured values were 0.98×10^{-12} A, measured 5 days after the processing was completed, and 1.3×10^{-12} A, measured 38 days later. These data are representative of time-dependent increases in the $n = 2$ current of 0.5-cm × 0.5-cm cells, which are attributed to changes in the surface condition of the GaAs. Such changes were also observed in [20]. Changes in the $n = 2$ current produce small changes in the fill factor of 0.5-cm × 0.5-cm cells, but should be less important in large-area 1-sun cells where the perimeter is less important or in concentrator cells operated at high intensities where the $n = 1$ current is dominant.

Deep-level transient spectroscopy (DLTS) measurements were made on small diodes from each wafer. The MOCVD wafers showed a single deep level, tentatively identified as EL2, at concentrations of 5.8×10^{13} cm^{-3} for wafer 15271 and 4.2×10^{13} cm^{-3} for wafer 15523. No deep levels were detected in the MBE material, with a detection limit of 1×10^{13} cm^{-3}.

IV. Discussion

A. Comparison of Growth Methods

Because the solar cell structure and device processing steps were nominally identical for both growth methods, a comparison of device results can be used to compare the material quality of MOCVD and MBE epitaxial layers. The conversion efficiencies of cells grown by both methods were very high. Both types of materials therefore have very high quality; the similarities outweigh the differences. However, there *were* some differences responsible for the one-percentage point efficiency difference between MOCVD and MBE cells, as pointed out in the following discussion.

The biggest difference between the MBE and MOCVD cells was in the fill factor. The fill factors of the MBE cells were lowered by nonideal dark currents with $n > 2$ (see Fig. 7); series resistances, however, were the same for both types of material. The excess leakage current appears to be related to discrete growth defects in the MBE films. Oval defects appear to be the most likely cause because they were present in both MBE wafers but not in MOCVD wafers, and their density was higher in the wafer with higher excess leakage currents. The fact that the $n > 2$ leakage was observed on all of the large-area MBE-grown cells but only sporadically in small-area diodes supports this hypothesis.

We note that oval defects in MBE films can have their origins in contaminants on the starting substrate or can be introduced by the MBE system [18], [22]. The wafers used in this work were cleaned in a different building than the one containing the MBE system for reasons of expediency during construction of a new laboratory. Although as much care as possible was taken to maintain a clean substrate, the majority of the oval defects are attributable to the starting substrate condition. Based on the work of others [18], [22], we expect that the oval defect density can be greatly reduced in the near future when class 100 clean-room conditions are employed for preparing the substrates.

Open-circuit voltages were limited almost entirely by bulk diffusion current for both materials, as seen in Fig. 7. The diffusion saturation currents, given in Table IV, were similar for MBE and MOCVD materials. This implies that the minority-carrier recombination properties, namely bulk lifetime and heteroface recombination velocities, which determine the diffusion saturation current, were similar for the two materials. Open-circuit voltages were slightly lower on average for the MBE cells, although the best MBE cells were as good as the best MOCVD cells from wafer 15271. The $n > 2$ leakage current which limited the fill factor also accounts for a small V_{oc} loss.

The MBE-cell short-circuit currents are just slightly lower than those for MOCVD cells. Similar spectral response curves indicate comparable (and very good) diffusion lengths and recombination velocities in both materials. Modeling of the spectral response curves indicates an emitter diffusion length more than three times the emitter thickness in all cases and a base diffusion length more than twice the base thickness for all cells except 15271-18, where the ratio was greater than 1.5. Heteroface recombination velocities are less than 4×10^4 cm/s in all cases at the front of the emitter and less than 4 ×

10^3 cm/s at the back of the base layer. These values, which are consistent with recent photoluminescence decay measurements of our MOCVD material [23], confirm that nearly all carriers are being collected from the emitter and base layers of the solar cells. The small difference in short-circuit current is attributed mostly to losses in the AlGaAs window layer, which was somewhat thicker and of a lower composition (lower bandgap) for the MBE cells.

In terms of uniformity and yield, MBE wafer 121588B had a higher spread in values across the wafer and a larger number of defective cells than the other three. We believe this to be caused by substrate-related growth defects. The other wafers, both MBE- and MOCVD-grown, demonstrated excellent uniformity in device characteristics across the 2-in wafers and nearly 100-percent yield of good devices.

In summary, the only significant difference between the two growth methods was the presence of isolated growth defects in the MBE material that increased the p-n junction leakage. The defects have not been thoroughly investigated, but the majority are attributable to the starting substrate cleanliness and should be easily eliminated as discussed above. Small differences in the thickness and composition of the AlGaAs window layer could easily be corrected in future work.

B. Effect of MOCVD Growth Temperature

The two MOCVD wafers compared different growth temperatures. Although the efficiencies were similar, there were differences favoring the higher growth temperature. The short-circuit current was marginally higher for the cells grown at 775°C and would have been even better with an antireflection coating identical to that of the cells grown at 740°C. The long wavelength response was higher for the cell grown at 775°C, suggesting a higher base diffusion length, although the thicker emitter and base layers for this sample were also a factor. The $n = 1$ diffusion saturation current was also lower, giving higher V_{oc} (see Fig. 7). Both results suggest higher diffusion lengths in the n-type Si-doped GaAs base layer when grown at higher temperatures. The DLTS data indicated a lower deep level concentration in the sample grown at the higher temperature, although not enough measurements were taken to be sure of the statistical significance of this.

V. Conclusions

We have found that comparable materials quality for photovoltaic applications can be achieved with state-of-the-art MBE- and MOCVD-grown GaAs solar cell structures. Very high efficiency cells have been fabricated on both types of materials. The best MOCVD cells have the highest independently confirmed efficiency (24.8 percent) ever reported for a single-junction solar cell at 1-sun terrestrial conditions. These are also the highest efficiency (23.8 percent) MBE-grown GaAs cells on record. The fill factors and efficiencies of the MBE-grown cells were limited somewhat by growth defects that introduced junction leakage. However, the minority-carrier transport properties were very similar for the two materials, showing that experimental results from MBE-grown cells should be applicable to the more widely used MOCVD technology.

Acknowledgment

The authors wish to acknowledge the expert technical assistance of T. Dixon, L. Geoffroy, C. Keavney, M. Jeanson, M. Josephson, W. Jarrett, M. Sanfacon, and L. Mitzman at Spire Corporation in the materials growth, device processing, and characterization of the solar cells. The authors wish to acknowledge the long-term financial support of this work by SERI (C. Leboeuf and J. Benner) as an important part of its success. M. R. Melloch would like to thank R. Chow, R. Fernandez, and G. Ross of Varian Associates for all their help and guidance in bringing up a new GEN II MBE system.

References

[1] S. P. Tobin and S. M. Vernon, "High efficiency GaAs and GaAs/Ge tandem solar cells," in *Tech. Dig. 4th Int. Photovoltaic Science Eng. Conf.* (Sydney, Australia) Feb. 14-17, 1989, pp. 865-872.

[2] K. A. Bertness, M. Ladle Ristow, and H. C. Hamaker, "High-efficiency GaAs solar cells from a multiwafer OMVPE reactor," in *Conf. Rec. 20th IEEE Photovoltaic Specialists Conf.* (Las Vegas, NV) Sept. 1988, pp. 769-770.

[3] R. P. Gale, R. W. McClelland, B. D. King, and J. V. Gormley, "High-efficiency thin-film AlGaAs-GaAs double heterostructure solar cells," in *Conf. Rec. 20th IEEE Photovoltaic Specialists Conf.* (Las Vegas, NV), Sept. 1988, pp. 446-450.

[4] C. Amano, M. Yamaguchi, and A. Shibukawa, "Optimization of radiation-resistant GaAs solar cell structures," in *Tech. Dig. 1st Int. Photovoltaic Science Eng. Conf.* (Kobe, Japan), 1984, pp. 845-848.

[5] A. Seletes *et al.*, "GaAlAs/GaAs solar cells grown by molecular beam epitaxy: Material properties and device parameters," *Solar Cells*, vol. 17, pp. 373-381, 1986.

[6] H. L. Chuang, P. D. DeMoulin, M. E. Klausmeier-Brown, M. R. Melloch, and M.S. Lundstrom, "Evidence for bandgap narrowing effects in Be-doped, p-p^+ GaAs homojunctions," *J. Appl. Phys.*, vol. 64, pp. 6361-6364, 1988.

[7] H. L. Chuang, M. E. Klausmeier-Brown, M. R. Melloch, and M. S. Lundstrom, "Effective minority carrier hole confinement of Si-doped, n^+/n GaAs homojunction barriers," *J. Appl. Phys.*, vol. 66, p. 273, 1989.

[8] M. R. Melloch, D. C. Miller, and B. Das, "Effect of a GaAs buffer layer grown at low substrate temperatures on a high-electron-mobility two-dimensional electron gas," *Appl. Phys. Lett.*, vol. 54, pp. 943-945, 1989.

[9] J. H. Neave, B. A. Joyce, P. J. Dobson, and N. Norton, "Dynamics of film growth of GaAs by MBE from RHEED observations," *Appl. Phys. A*, vol. 31, pp. 1-8, 1983.

[10] T. J. Drummond *et al.*, "Use of a superlattice to enhance the interface properties between two bulk heterolayers," *Appl. Phys. Lett.*, vol. 42, pp. 615-617, 1983.

[11] K. L. Tan, M. S. Lundstrom, and M. R. Melloch, "Effect of impurity trapping on the capacitance-voltage characteristics of n-GaAs/N-AlGaAs heterojunctions," *Appl. Phys. Lett.*, vol. 48, pp. 428-430, 1986.

[12] S. P. Tobin *et al.*, "Device processing and analysis of high efficiency GaAs solar cells," *Solar Cells*, vol. 24, pp. 103-115, 1988.

[13] S. P. Tobin, M. B. Spitzer, C. Bajgar, L. Geoffroy, and C. J. Keavney, "Advanced metallization for highly efficient solar cells," in *Conf. Rec. 19th IEEE Photovoltaic Specialists Conf.*, 1987, pp. 70-75.

[14] *Standard for Terrestrial Spectral Solar Spectral Irradiance Tables at Air Mass 1.5 for a 37° Tilted Surface*, ASTM Standard E892-87, 1988; also in R. Hulstrom, R. Bird, and C. Riordan, "Spectral solar irradiance data sets for selected terrestrial conditions," *Solar Cells*, vol. 15, pp. 365-391, 1985.

[15] K. A. Emery and C. R. Osterwald, "Solar cell efficiency measurements," *Solar Cells*, vol. 17, pp. 253-274, 1986.
[16] P. Blood, "Capacitance-voltage profiling and the characterisation of III-V semiconductors using electrolyte barriers," *Semicond. Sci. Technol.*, vol. 1, pp. 7-27, 1986.
[17] M. M. Sanfacon and S. P. Tobin, "Analysis of AlGaAs/GaAs solar cell structures by optical reflectance spectroscopy," *IEEE Trans. Electron Devices*, this issue, 450-454.
[18] A. Salokatve, J. Varrio, J. Lammasniemi, H. Asonen, and M. Pessa, "Reduction of surface defects in GaAs grown by molecular beam epitaxy," *Appl. Phys. Lett.*, vol. 51, pp. 1340-1342, 1987.
[19] P. D. DeMoulin, S. P. Tobin, M. S. Lundstrom, M. S. Carpenter, and M. R. Melloch, "Influence of perimeter recombination of high-efficiency GaAs p/n heteroface solar cells," *IEEE Electron Device Lett.*, vol. 9, pp. 368-370, 1988.
[20] C. H. Henry, R. A. Logan, and F. R. Merrit, "The effect of surface recombination on current in $Al_xGa_{1-x}As$ heterojunctions," *J. Appl. Phys.*, vol. 49, pp. 3530-3542, 1978.
[21] J. S. Blakemore, "Semiconducting and other major properties of gallium arsenide," *J. Appl. Phys.*, vol. 53, pp. R123-R181, 1982.
[22] S.-L. Weng, C. Webb, Y. G. Chai, and S. G. Bandy, "Particulates: An origin of GaAs oval defects grown by molecular beam epitaxy," *Appl. Phys. Lett.*, vol. 47, pp. 391-393, 1985.
[23] R. K. Ahrenkiel *et al.*, "Ultralong minority-carrier lifetime epitaxial GaAs by photon recycling," *Appl. Phys. Lett.*, vol. 55, pp. 1088-1090, 1989.

*

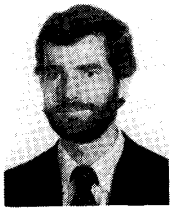

Stephen P. Tobin (S'78-M'79) received the S.B. and S.M. degrees in electrical engineering from the Massachusetts Institute of Technology in 1979.

From 1975 to 1980, he was involved in the development of HgCdTe photovoltaic infrared detectors at the Honeywell Electro-Optics Center. He joined Spire Corporation in 1980 where he is presently a Staff Scientist. His research group has developed a wide variety of high-efficiency solar cells in silicon and III-V materials systems. His present interests include improving the conversion efficiency of epitaxial GaAs solar cells on GaAs, silicon, and germanium substrates.

*

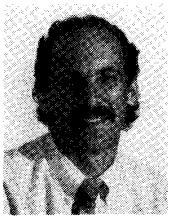

Stanley M. Vernon received the B.S. degree in physics from Boston College in 1972 and the M.S. degree in electrical engineering in 1976 from Rutgers University where his thesis work involved the study of Schottky-barrier solar cells.

From 1976 to 1981, he was employed at IBM's Thomas J. Watson Research Center where he performed research on metalorganic chemical vapor deposition (MOCVD) of GaAs for solar cell and transistor applications. Since 1981, he has worked at Spire Corporation where he is now Manager of MOCVD Research. In this capacity he directs numerous programs concerning the growth of thin-film semiconductor structures. His special areas of expertise involve heteroepitaxial and high-efficiency-photovoltaic materials; many of his current research activities are in the realm of depositing compound semiconductors onto Si substrates. He also established Spire's MOCVD Equipment and III-V Epitaxial business units; he currently advises those groups in technical issues.

*

Clara Bajgar received the M.S. degree in physics from Komensky University in Bratislava, Czechoslovakia, in 1967.

She worked as a Physicist for New England Nuclear Corporation before joining Spire Corporation as a Staff Scientist in 1977. Her activities and interests include device fabrication in GaAs and Ge and high-temperature metallization of GaAs solar cells.

Steven J. Wojtczuk (S'84-M'87) received the B.S. degree in electrical engineering with highest honors from Rutgers University in May 1980 and the Ph.D. degree from Cornell University in May 1987 for research on high-speed GaAs/AlGaAs photodetectors and monolithically integrated photoreceivers. He held an RCA fellowship (1980) and was an Eastman Kokak Fellow (1981-1984) while at Cornell.

He has worked at Honeywell's Electro-Optics Division on HgCdTe long-wavelength infrared arrays and high-speed potodiodes for coherent detection. In 1988, he joined Spire Corporation, where he is investigating GaAs/Ge tandem solar cells and AlGaAs superlattice long-wavelength detectors.

Dr. Wojtczuk is a member of Eta Kappa Nu and Tau Beta Pi.

*

Michael R. Melloch (S'80-M'82) was born in Hammond, IN, in 1953. He received the B.S.E.E., M.S.E.E., and Ph.D. degrees from Purdue University in 1975, 1976, and 1981, respectively.

From 1976 to 1978 he was a Design Engineer at Intel Corporation, Santa Clara, CA. In 1982 he joined the Central Research Laboratories at Texas Instruments as a Member of the Technical Staff. At Texas Instruments his research interests centered around GaAs surface acoustic wave devices. In 1984 he joined the School of Electrical Engineering, Purdue University, as an Assistant Professor and is presently an Associate Professor there. Currently he is engaged in research related to molecular beam epitaxy and III-V device structures.

Dr. Melloch is a member of Tau Beta Pi, Phi Kappa Phi, Sigma Pi Sigma, and the American Physical Society.

*

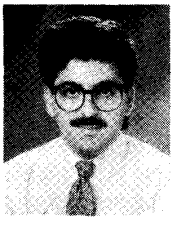

Ali Keshavarzi was born in Tehran, Iran, on September 5, 1964. He received the B.S. degree in electrical engineering from the University of Tennessee at Knoxville in 1987. He is currently working toward the master's degree at Purdue University in solid-state materials and devices. His research involves the basic studies of III-V crystalline cell components, especially development of high efficiency MBE-grown AlGaAs solar cells.

*

Theresa B. Stellwag was born in Newport News, VA, in 1966. She received the B.S.E.E. degree from Virginia Polytechnic Institute and State University in 1988. She is currently completing the M.S. degree at Purdue University. Her research involves the characterization of recombination losses in GaAs p/n diodes.

*

S. Venkatensan, photograph and biography not available at time of publication.

Mark S. Lundstrom (S'80-M'80) was born in Alexandria, MN, in 1951 and received the B.E.E. degree with high distinction from the University of Minnesota in 1973. He was awarded the M.S.E.E. degree from the University of Minnesota in 1974 for thesis research on magnetoelastic surface acoustic wave devices. In 1980 he received the Ph.D. in electrical engineering from Purdue University for research on silicon solar cells.

Since 1980 he has been a member of the faculty at Purdue University where he is presently Professor of Electrical Engineering and Director of the Optoelectronics Research Center. From 1974 to 1977 he was employed by Hewlett-Packard Corporation where he worked on NMOS integrated circuit process development and manufacturing. His research now centers on heterostructure device physics, with emphasis on heterostructure solar cells and bipolar transistors. He is presently engaged in developing and applying techniques for numerically simulating heterostructure devices and in experimental research on minority carrier injection, transport, and recombination in III-V heterostructures.

*

Keith A. Emery (S'80-M'80) photograph and biography not available at the time of publication.